

Validation of Predicted Vibratory Loads of a Coaxial Rotor at High Advance Ratios with Wind Tunnel Test Data

Joseph Schmaus
PhD student

Inderjit Chopra
Alfred Gessow Professor
Distinguished University Professor
Director

Alfred Gessow Rotorcraft Center, University of Maryland
College Park, Maryland, United States

Abstract

The predictions of a comprehensive analysis based on UMARC are compared to experimental coaxial rotor results. The experiments cover a range of collective pitch angles (θ_o) from 2° to 10° , advance ratios (μ) from 0.2 to 0.5, and lift offset from 0% to 20%. The experimental model rotor system is a pair of hingeless coaxial rotors, with two blades each, and a first flap frequency of approximately 1.6/rev. It was tested in the Glenn L. Martin Wind Tunnel at the University of Maryland as isolated rotors and as a counter-rotating coaxial rotor system. The simulation is validated against coaxial performance and vibratory loads. The simulation captures increasing rotor efficiency with lift offset and advance ratio and also properly models 2/rev vibratory loads with advance ratio, lift offset, and rotor-to-rotor phase. The inversion of thrust between upper and lower rotor with advance ratio is identified.

1. NOTATION

A	Rotor disk area, πR^2
c	Rotor reference chord, m
C_{l_α}	Lift curve slope
C_F	Force coefficient, $F/\rho A \Omega^2 R^2$
C_M	Moment coefficient, $M/\rho A \Omega^2 R^3$
I_b	Blade flap inertia, kg m ²
L/D_e	Lift-to-drag ratio, $C_T/(C_Q/\mu + C_X)$
LO	Lift offset, $2C_{M_x}/(C_T^U + C_T^L)$
m_o	Mass per length, kg/m
N_b	Number of blades
R	Rotor radius, m
β_p	Precone, degrees
γ	Lock number, $\rho C_{l_\alpha} c R^4 / I_b$
θ_o	Collective, degrees
θ_{1c}	Longitudinal control angle, degrees
θ_{1s}	Lateral control angle, degrees
μ	Advance ratio, $V_{tunnel}/\Omega R$
ρ	Air density, kg/m ³
σ	Rotor solidity, $N_b R c / \pi R^2$
ϕ	Rotor-to-rotor phase angle, degrees
Ω	Rotor rotational speed, rad/s



Figure 1: UT Austin model rotor in the Glenn L. Martin Wind Tunnel.

2. INTRODUCTION

Next generation vertical lift configurations will be required to fly faster than current helicopters while maintaining excellent low speed efficiency. These two at-

tributes are traditionally in competition, but the Future Vertical Lift (FVL) and the DARPA VTOL X-Plane projects seek to merge the two. Among the viable concepts that meet these goals is the high speed coaxial helicopter, of which Sikorsky has developed a series of successful technology demonstrators. The goal of this paper is provide insight into the aeromechanics of this configuration. To achieve this goal, a robust and validated comprehensive analysis for counter-rotating coaxial rotors is developed and it is used to evaluate a model rotor being developed for wind tunnel testing.

Coaxial rotors have been used in many helicopters because the reaction torque is handled in a compact design, including several models by Kamov and the QH-50 DASH. Early studies of coaxial rotors focused on hover performance and articulated hubs with large rotor spacing. Harrington [1] and Dingeldein [2] studied performance of an early coaxial helicopter in hover and forward flight, comparing it with similar isolated rotors. Coleman [3] summarized these experiments as part of a larger paper that included all coaxial experimental results performed up to 1997, noting the common observation that in hover coaxial rotors have slightly improved performance over isolated rotors with similar solidity. More recently Ramasamy [4] performed a set of experiments on small scale two-rotor systems, illustrating the differences between coaxial, tandem, and tilt rotors.

Modern high speed coaxial helicopters require modifications that differentiate them from traditional coaxial helicopters. These include stiff, hingeless rotor blades and auxiliary propulsion that allow them to leverage the advantages of a lift offset rotor while keeping the rotor spacing to a minimum. Sikorsky's technology demonstrators, the XH-59A and the X2, have demonstrated this is a viable configuration for high-speed flight. Ruddell [5] summarized the development and flight testing of the XH-59A. Blade loads are also available from wind tunnel tests [6]. Unfortunately, gaps in the documentation of the experimental method have made this data difficult to use for validation. The X2 completed a series of flight tests, culminating in a flight of 250 kts in steady level flight in 2010 [7, 8].

Analysis techniques for coaxial rotors have expanded significantly since Harrington [1] suggested that equivalent single rotor solidity was sufficient to model the performance of a coaxial helicopter. Leishman [9] and Johnson [10] presented momentum theory derivations that treat the two rotors as separate but incorporate the contracted wake from the upper rotor on the lower rotor. This captures interactions between the two rotors, but is dependent on prescribed contraction ratios and skew angles at high advance ratio. Further studies have compared blade element momentum theory [11] with free-vortex wake

and computational fluid dynamics (CFD) results [12], showing satisfactory correlation between all three fidelity methods in hover. Yeo and Johnson [13] used CAMRAD II to study the impact of lift offset on rotorcraft performance. They highlighted the increase in the stall boundary when lift offset is used and enumerated the importance of proper twist and taper. Johnson, Moodie, and Yeo [14] performed an iterative design study highlighting the importance of hub drag and rotor weight on the design of a high speed coaxial helicopter. Hovering performance of coaxial rotors was examined with CFD [15, 16], and showed promise in performance prediction as well as improve prediction of vibrations that result from the interaction between blades as they cross. Passe, Sridharan, and Baeder [17] estimated performance and interactional aerodynamics of a hypothetical X2 in forward flight using CFD. They predicted larger interactions between upper and lower rotor than in the baseline lifting line analysis.

A hingeless, coaxial, model rotor has been developed by the University of Texas at Austin (UT Austin), Figure 1. Hover performance of this test stand is described by Cameron, Uehara, and Sirohi [18]. The rotor was tested in July and October 2015 in the Glenn L. Martin Wind Tunnel at the University of Maryland (UMD), described in detail by Cameron and Sirohi [19]. The first wind tunnel entry explored isolated rotor performance and tested hardware integration for a blade-to-blade clearance sensor. The second entry included a range of tests examining isolated rotor, coaxial rotor, RPM variation, and phasing between the rotors.

A comprehensive analysis has been developed taking University of Maryland Advanced Rotor Code, UMARC [20], as a baseline platform. This analysis has been used to predict rotor tip clearances and loads to aid in successfully performing tests over a complete flight envelope in the wind tunnel [21]. The authors used the current analysis to explore the performance of the isolated rotors in detail and examine preliminary coaxial vibratory correlations [22]. The current work focuses on coaxial performance and loads, seeking to identify the results of aerodynamic interaction.

2.1. Lift Offset

The primary advantage of a coaxial rotor in high speed coaxial helicopters is the ability to leverage lift offset. Figure 2a shows a typical lift distribution on an untwisted rotor at high advance ratio without lift offset. The maximum lift on the retreating side is higher than the advancing side and, to maintain roll balance, the advancing side generates negative lift over more than half the span. Figure 2b shows a similar coaxial rotor that has been trimmed with lift offset, allowing each

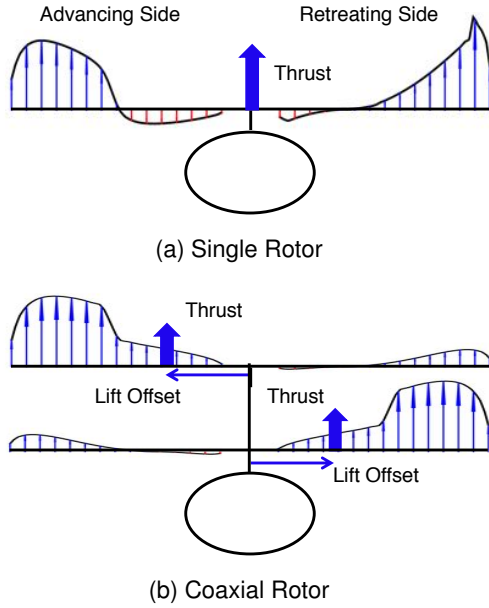


Figure 2: Lift distribution on a rotor without lift offset (a) and with lift offset (b)

rotor to generate a roll moment reacted against each other. The efficiency of the rotor has been increased by reducing stall on the retreating side and allowing the entire advancing side to generate positive lift.

In a coaxial system, the upper and lower rotor do not necessarily carry the same thrust, so to maintain roll balance, lift offset is defined based on the average rotor thrust.

$$(1) \quad LO = \frac{2C_{M_x}}{C_T^U + C_T^L}$$

In Equation (1), C_{M_x} is the hub rolling moment coefficient. C_T^U and C_T^L are the thrust coefficients for the upper and lower rotors, respectively.

3. METHOD

3.1. Model Rotor

The model rotor being studied in this paper was designed and fabricated by UT Austin for testing in the Glenn L. Martin Wind Tunnel at UMD. It is a hydraulic powered, belt driven, hingeless rotor system that can have either isolated or coaxial rotors with two or four blades on each rotor. The two-bladed coaxial rotor system in the wind tunnel is shown in Figure 1. The upper rotor spins in the counter-clockwise direction when seen from above while the lower rotor spins clockwise.

The rotor blades are untwisted, have uniform chord and use a modified VR-12 airfoil. The root of each blade is reinforced with a structural fairing that ex-

Table 1: Model Rotor Characteristics.

Property	Value
Radius	1.016 m
N_b	2
Solidity, σ	0.10
Tip speed	96 m/s
Twist	0°
Rotor Separation	13.8% R
Lock Number, γ	5.9
Precone, β_p	3°

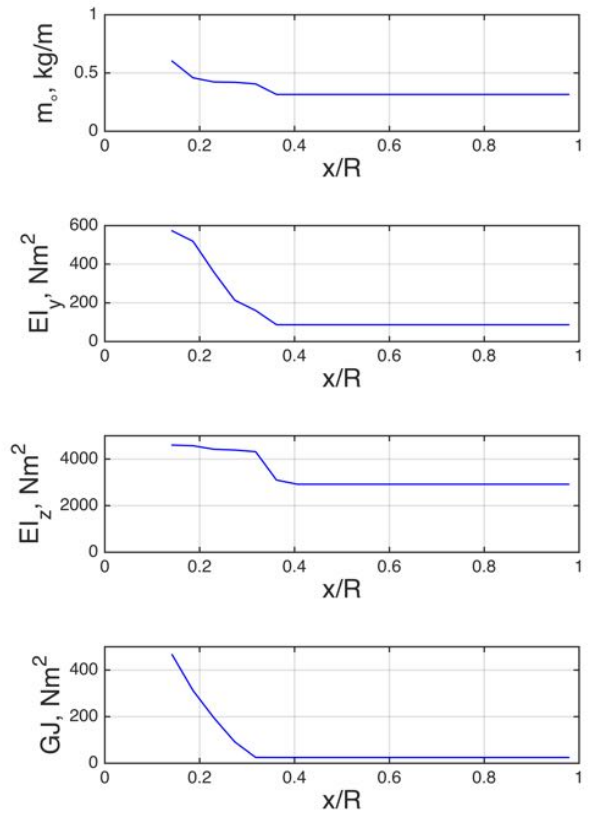


Figure 3: Rotor blade spanwise structural properties.

tends to 35% of the span. The fairing reduces the aerodynamic impact of the blade grip, smoothly transitioning to the primary airfoil shape. It is also designed to increase the blade stiffness. Some key geometric parameters of the rotor are included in Table 1. The design rotor speed was 188 rad/s but in practice tests were mostly performed at 94 rad/s. The blade structural properties are displayed in Figure 3. Each rotor had a different control system geometry, described in detail previously by the authors [22]. Table 3 summarizes the pushrod stiffness and pitch horn length for the different rotors.

The details of the experimental setup are described by Cameron and Sirohi [19]. Data that were recorded

Table 2: Experimental test envelope.

Configuration	RPM	Advance Ratio	Collective, deg	Lift Offset, %
Lower Rotor	900	0.2,0.3,0.4,0.5	3,5,8,10	0,5,10,15,20
Upper Rotor	900	0.2	3,5,8,10	
		0.2	3,5,8	
		0.4,0.5	2,4,6,8	
Coaxial Rotor	900	0.2,0.3,0.4,0.5	2,4,6,8	
	1200			
Coaxial Rotor ($\phi = 20^\circ, 45^\circ$)	900	0.2,0.3	4,6	

include rotating frame hub loads, blade root pitch angle, pitch link forces, blade tip clearance, rotor RPM and tunnel speed. Each experimental point is a phase average of 100 sequential revolutions. In all cases, non-dimensional rotor forces in this paper are calculated using the time averaged rotor speed for the current test point. The given advance ratio also takes into account the measured tunnel speed. A study was carried out to examine the impact of rotor-to-rotor phases. The upper and lower rotors are driven by a toothed belt that prevented slipping and it was regularly confirmed that the phase did not change during tests.

Table 3: Model Rotor Pushrod Properties.

Property	Upper Rotor	Lower Rotor
Length	0.013 m	0.023 m
Stiffness	7.0×10^5 N/m	7.3×10^5 N/m

The flight envelope encompassed several collectives, advance ratios, and lift offsets. Table 2 shows a full range of collectives and advance ratios tested. For each point in the test envelope, test points were taken across a full range of lift offset values, up to 20%. All experiments were taken with a physical shaft angle of 0° .

3.2. Airfoil Tables

The VR-12 is a valuable airfoil for helicopters because it has superior low Mach number performance and a high drag divergence Mach number [9]. Joining the upper and lower skin of the airfoil creates a 0.0038m tab at the rear of the airfoil, approximately the trailing edge 5% of the chord, Figure 4. The presence of this trailing edge tab changes the airfoil properties, most notably the pitching moment.

Computational Fluid Dynamics (CFD) is used to evaluate the aerodynamic changes from the baseline VR-12 airfoil. TURNS was used as described by Srinivasan and Baeder [23]. TURNS is a time-accurate structured Reynolds-Averaged Navier–Stokes solver, formulated using a dual-volume finite difference approach. The Spallart–Almaras turbulence model was

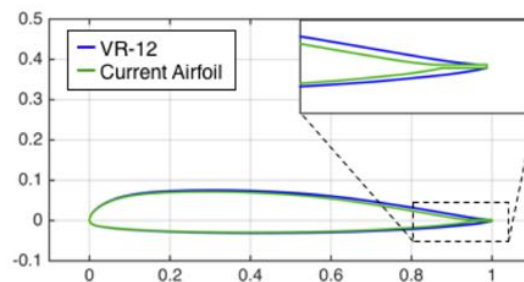


Figure 4: Comparison between a true VR-12 airfoil and the modified airfoil with the trailing edge tab used in this study.

used along with a transition model that more accurately predicts the laminar-turbulent transition of the boundary layer [15]. An O-mesh was used for the modified VR-12 airfoil, with a wall spacing of 10^{-5} . The Mach number range of interest is 0.1–0.5 and the related Reynolds numbers 1.67×10^5 – 8.33×10^5 . Figure 5 shows the lift drag and pitching moment curves for a selection of Mach numbers.

3.3. UMARC

The simulation results in this paper are performed with a modified version of UMARC that allows for coaxial rotor solution. Baseline UMARC models the blades as second order, nonlinear isotropic Euler-Bernoulli beams capable of undergoing coupled flap, lag, torsion, and axial motion. Performance and loads prediction is carried out using a Wessinger-L lifting line theory and time accurate free-wake to capture the effects of the far-wake. Airfoil properties are determined by full 360 degree, CFD enhanced, look-up tables.

This baseline model is expanded in a number of ways. The free-vortex wake solves the coupled coaxial rotor solution and captures rotor-to-rotor interactions of the tip vortices [24]. In this analysis, the bound vorticity of each blade, which is neglected in the inflow calculations of classical Bagai-Leisman free-wake, contributes to the inflow on every other blade. Further study is merited to improve this model,

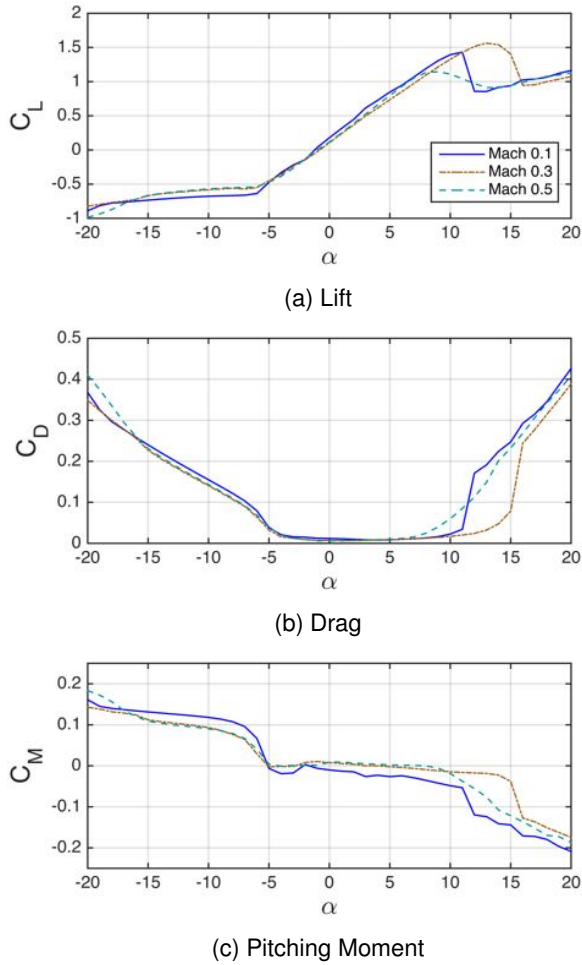


Figure 5: Airfoil properties for the modified VR-12 airfoil.

but it was seen to improve 4/rev hub load correlations. Rotor wake and hub loads calculations are expanded to allow for rotors with relative phase offset. Provisions are made for each rotor to have separate structural properties. Trim routines allow for a number of configurations, including (but not limited to) trimming to zero first harmonic flapping based on root angle or tip displacement. Trim controls for each rotor can either be coupled or decoupled based on the desired application and control scheme. The near-wake is used in the reverse flow region, has a prescribed deformation based on the local flow, and it is allowed to reverse directions.

3.4. Simulation Parameters

The simulation models the rotor system using 20 evenly spaced structural elements, and 12 finite elements in time using 5th order Hermite time shape polynomials. A modal reduction is performed using the first ten coupled rotating modes, this includes two

lag, five flap, and three torsion modes. A single modified VR-12 airfoil is used along the entire span of the blade, this neglects the aerodynamic impact of increasing thickness at the root. Modal damping is set at 2% for all modes. An aerodynamic and structural root cutout extends to 12% of the rotor radius. The aerodynamic model includes tabulated reverse flow aerodynamics. The far-wake model is based on the Bagai-Leishman [24] free-vortex wake model with a ten degree discretization and a single tip trailer per blade. In hover, six full turns of the wake are used, while in forward flight two turns provide significant computational improvements without modifying the vibratory loads.

Coaxial simulations use a five degree of freedom trim, with the upper rotor collective prescribed, while the lower rotor collective is free to vary. The lateral and longitudinal cyclic of each rotor are treated independently. The relevant residuals are pitch and rolling moments for each rotor and total system torque balance. When comparisons are shown with respect to a single specific data point, each rotor thrust, pitching and rolling moment are targeted and the upper rotor collective is allowed to vary. Isolated rotor wind tunnel trim is performed by a two degree of freedom trim, setting the collective at the desired value and trimming lateral and longitudinal cyclic so that target pitching and rolling moments are achieved. A correction is applied to the rotor shaft angle based on total system thrust and tunnel speed [25], although for the flight conditions studied, this never exceeded 1° nose up shaft tilt.

4. VALIDATION

4.1. Fan Plot

The upper and lower rotor have identical structural properties other than the pitch horn length. Figure 6 shows the fanplots for the upper and lower rotor overlaid on top of each other. The pitch horn for the lower rotor is longer than the upper rotor, so the lower rotor has a stiffer effective root spring. The resulting torsional frequencies of the upper and lower rotors are approximately 7.06/rev and 9.59/rev respectively, see Table 4. The second flap mode is close to 7/rev at the operational rpm. During the testing, fixed frame vibratory loads identified a resonance and the operational RPM was raised slightly above 900 to move from this resonance condition.

Experimental non-rotating natural frequencies are shown with the symbols along the axis. Flap and lag modes match well with the given properties. Torsion matches when pitch link stiffness is infinite (not shown), but the simulation was regularly performed including pitch link flexibility.

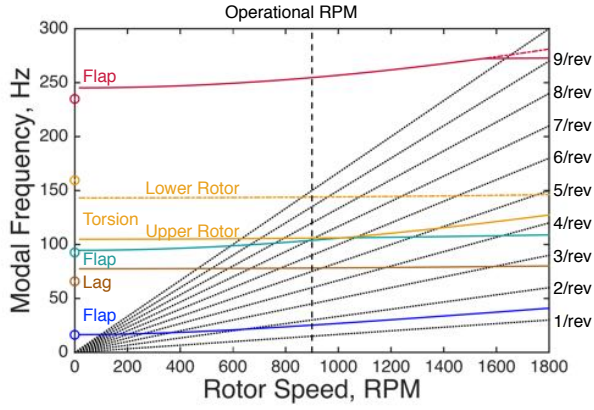


Figure 6: Upper and lower rotor fan plots. The upper rotor is solid, while the lower rotor is dashed.

Table 4: Modal Frequencies.

Mode	Rotor	50% 900 RPM	100% 1800 RPM
1-Flap	Both	1.66/rev	1.35/rev
2-Lag	Both	4.45/rev	2.28/rev
3-Flap	Both	6.73/rev	4.14/rev
4-Torsion	Upper	7.06/rev	3.63/rev
	Lower	9.59/rev	4.87/rev

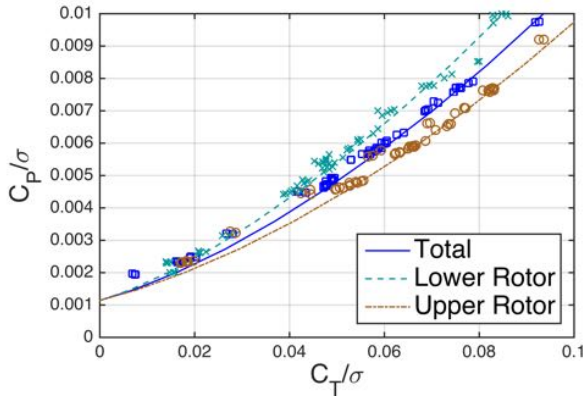


Figure 7: Hover stand performance compared with simulation.

4.2. Hover Performance

Isolated and coaxial rotor hover tests were performed using the rotor test stand on a hover tower at the University of Texas at Austin [18]. Figure 7 shows correlation between the UMARC prediction of hover power compared with the experiment for a coaxial with 2 blades on each rotor. The experiment and the simulation agree well with each other, suggesting that both the baseline airfoil tables and the free-wake are performing adequately. Both the experiment and the sim-

ulation were trimmed until the torque from each rotor was equal and opposite. As has been observed extensively in the past, the upper rotor has better performance than the lower rotor. This is a result of the lower rotor operating in the wake of the upper rotor while the upper rotor has relatively clean inflow. The resulting total coaxial performance is an average of each rotor.

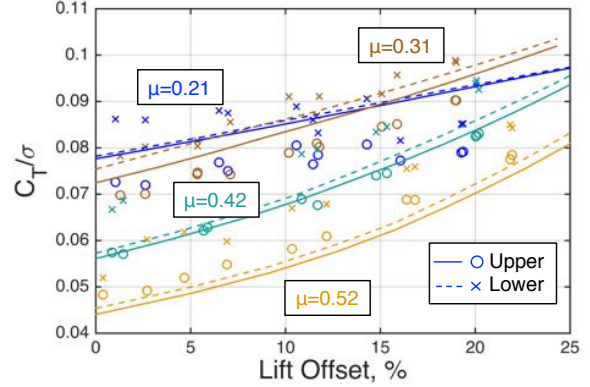


Figure 8: Individual rotor thrust from coaxial experiments plotted against lift offset for a number of advance ratios ($\theta_o = 6^\circ$).

5. RESULTS

5.1. Performance

Rotor performance is explored here by keeping collective constant at 6° because performance trends vary more with lift offset and advance ratio than collective. Rotor performance is evaluated through several parameters, including thrust shown in Figure 8. The x-axis is lift offset and the y-axis is thrust. The simulation captures the overall behavior of the experiment. Two dominant trends are evident. The first is that, for constant collective, increasing lift offset increases thrust. Second, increasing advance ratio decreases thrust. The second trend is a well established property of rotors tested in a wind tunnel and is related to thrust reversal at high speed. Another trend is the difference in slope with advance ratio for the lowest speed case, $\mu = 0.21$. Using lift offset allows the rotor to operate in a natural asymmetry, reducing the lift requirements on the side that has low dynamic pressure and reverse flow. However, at low advance ratio the rotor has little asymmetry, and therefore does not benefit as significantly from the application of lift offset. It is also evident that the lower rotor tends to produce more thrust than the upper rotor, this is a trend that is captured in both the experiment and the simulation, although the magnitude of this difference is not

captured by the simulation. The following section will explore this in more detail.

Rotor torque is presented in Figure 9, shown against the same variables as thrust (Figure 8). The simulation correlates less with the experiment than does the thrust, although the general trends are captured. The torque is much less sensitive to lift offset than thrust. As the lift offset increases there is a small reduction of torque until a lift offset is reached and torque begins to increase. The point where this occurs is at higher lift offset for higher speeds. This trend is more clear in the simulation data than in the experiment, although it can be observed that the slope of the experimental points with lift offset does tend to decrease with increasing advance ratio. There is less scatter between the upper and lower rotor in this data because matching torque was one of trim conditions.

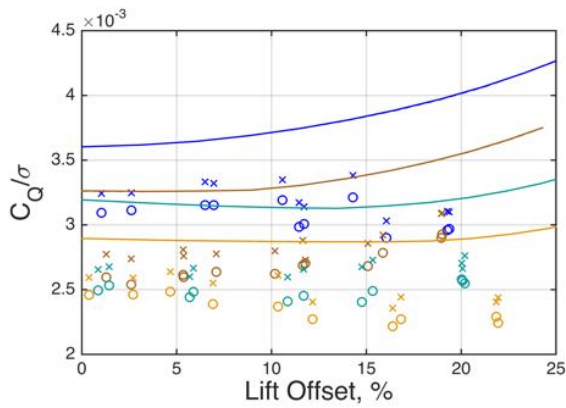


Figure 9: Individual rotor torque from coaxial experiments plotted against lift offset for a number of advance ratios ($\theta_0 = 6^\circ$).

Drag as a function of advance ratio and lift offset is shown in Figure 10. The trends are intriguing here, the increase in drag with lift offset is much more pronounced than it is in the rotor torque. However, with increasing advance ratio the slope of drag with lift offset decreases, even though thrust is going up. Hub drag is a result of many factors, including an asymmetry in sectional drag between the advancing and retreating sides. It can be increased by increasing drag on the advancing side or decreasing it on the retreating side. In this case, lift offset improves the efficiency of the retreating side, increasing the resultant hub drag. This trend is less pronounced at high speeds because dynamic pressure is lower on the retreating side where this effect occurs.

Rotor lift to drag ratio is a measure of the total efficiency of the rotor. It includes contributions from rotor thrust, profile power and torque. In non-dimensional

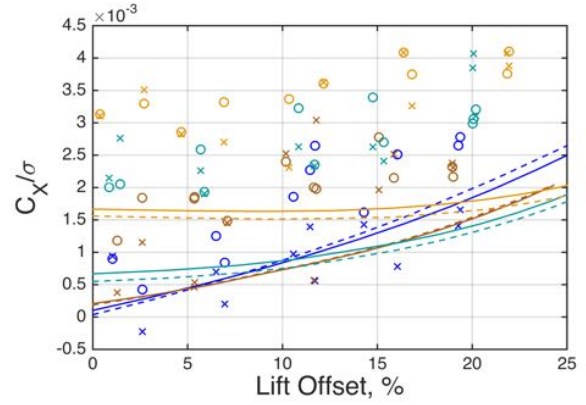


Figure 10: Individual rotor drag from coaxial experiments plotted against lift offset for a number of advance ratios ($\theta_0 = 6^\circ$).

form, it is represented as:

$$(2) \quad L/D_e = \frac{C_T}{\frac{C_Q}{\mu} + C_{M_x}}$$

Lift to drag ratio is unlike figure of merit, it is the same whether the coaxial system is defined as two rotors with equal area or one rotor with double solidity. The current simulation generally under-predicts the thrust and over-predicts the torque, which yields an L/D_e that is slightly under-predicted. The increasing thrust and relatively stable torque means that lift to drag ratio tends to increase with lift offset. It can be seen that the increasing drag with lift offset eventually decreases lift to drag ratio.

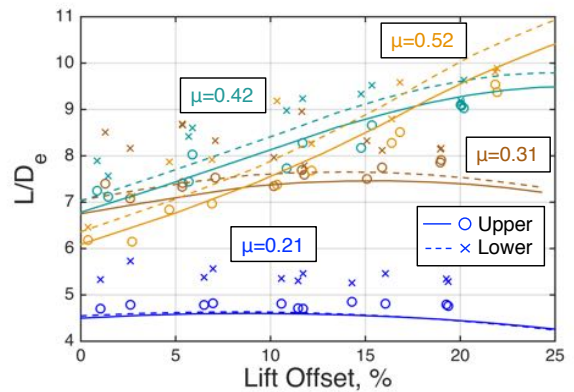


Figure 11: Individual rotor lift to drag ratio from coaxial experiments plotted against lift offset for a number of advance ratios ($\theta_0 = 6^\circ$).

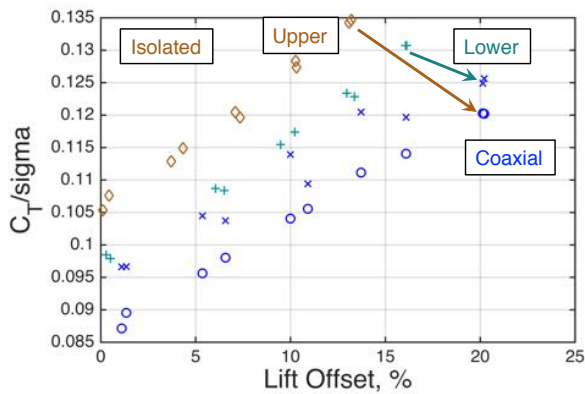


Figure 12: Thrust comparison between rotors run isolated and coaxial rotors ($\theta_o = 8^\circ$; $\mu = 0.31$).

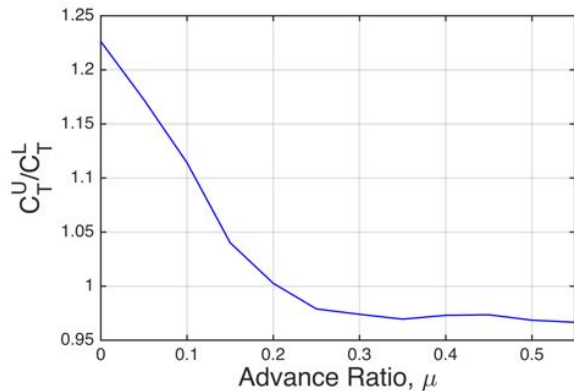


Figure 13: Ratio of upper to lower rotor thrust plotted against advance ratio, from the simulation ($\theta_o = 8^\circ$).

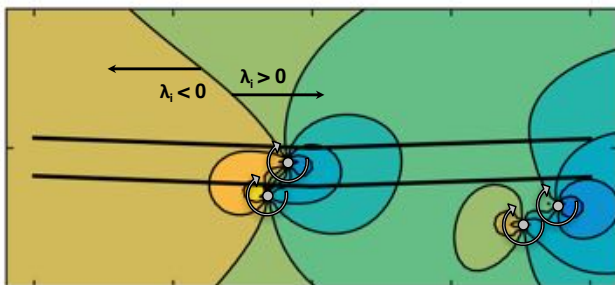


Figure 14: Vertical component of the far-wake induced inflow in the $x-z$ plane for $\psi = 0^\circ$ ($\theta_o = 8^\circ$; $\mu = 0.31$).

5.2. Comparison with Isolated

The authors' previous work presented a detailed comparison of isolated rotor performance [22]. It is instructive to see how the isolated rotor performance compares with the coaxial rotor. A collective of 8° is selected because data is available for both isolated rotors, whereas 6° is limited to data for the upper rotor only.

Figure 12 shows how experimental thrust varies with lift offset at an advance ratio of $\mu = 0.31$ for isolated and coaxial rotors. For the isolated rotor, it is expected that each rotor would produce similar thrust, however the upper rotor produces more thrust than the lower rotor. While it is not included here, the isolated upper rotor also has lower torque. Overall this means that while the rotors were manufactured to be identical, the upper rotor is significantly more efficient than the lower rotor when tested individually.

For the coaxial system, torque is balanced, so the relative efficiency of each individual rotor can be judged by the thrust alone. The lower rotor has become more efficient than the upper rotor. This trend of thrust inverting is consistently seen throughout the experimental data, and is surprising because of the markedly higher efficiency of the isolated upper rotor. This is also intriguing, because in hover, the upper rotor produces more thrust because of the interference on the lower rotor (Figure 7). Figure 13 shows how the simulation predicts the ratio of upper to lower rotor thrust changes with advance ratio. In hover the upper rotor produces a majority of the thrust, while after $\mu = 0.21$ the thrust inverts and the lower rotor produces more thrust.

Isolating the source of this thrust inversion is challenging because the wake development is complex and inherently coupled to the rotor loading. Figure 14 shows a longitudinal slice of the inflow induced from the rotor free-wake (not including near-wake induced inflow or the free stream). Two behaviors of the wake can be identified from this graph. First, while the wake induced inflow is generally negative, proximity to the left-hand side of the displayed vortices can reduce the induced inflow, or even make it a slight positive. Second, the interactions between the two wakes causes the upper rotor wake to convect downstream more quickly than the lower rotor wake, while both tend to move downward. It is theorized that the lower rotor therefore sees more reduction to the average inflow from the proximity to the vortex pairs, while this interaction is reduced on the upper rotor. The theory is challenging to verify because this interaction is subtle, it only accounts for a 5% difference in the thrust between the upper and lower rotor. Furthermore, the wake geometry is made significantly more complicated when the full 3-dimensional geometry is considered.

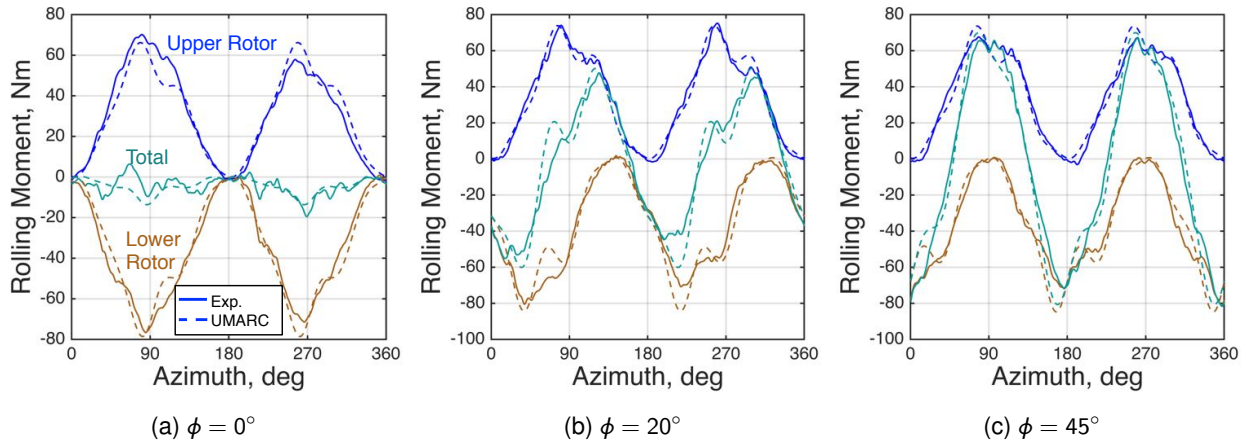


Figure 15: Resulting coaxial rolling moment time histories. ($\mu = 0.31$; $\theta_o = 6^\circ$; Lift Offset $\approx 15\%$)

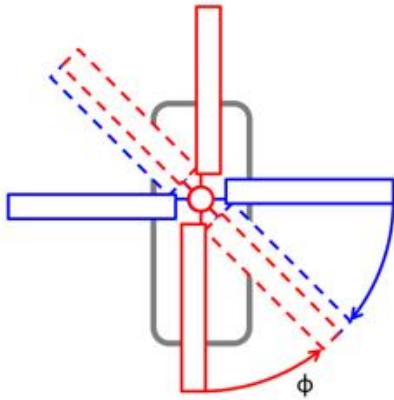


Figure 16: Definition of phase angle, ϕ .

5.3. Coaxial Hub Loads

Total coaxial rotor hub loads are dependent on a larger set of factors than traditional single rotors. In addition to normal flight condition parameters, there are also the following parameters:

- Application of lift offset
- Aerodynamic interactions between the upper and lower rotor
- Geometry of the coaxial system, specifically rotor-to-rotor phase (ϕ)

Figure 15 shows how the total rolling moment is a combination of the rolling moment from the upper and lower rotor. Figure 15a is a characteristic rolling moment distribution for a high lift offset. The experiment is shown with solid lines and the simulation is shown with the dotted line. Figure 15b and Figure 15c show

the same basic data but for rotors with different rotor-to-rotor phase angle, (ϕ defined in Figure 16). It is possible to see how the phase angle changes the resulting load, where for a phase angle of 45° , the rolling moment vibrations go from small to twice the isolated loads. The baseline rotor phase used throughout this paper is $\phi = 0$, the rotors pass over each other over the tail of the helicopter, excursions from this are discussed in a following section. Data taken at different rotor phase angles was limited to 4° and 6° collective and advance ratios of 0.2 and 0.3, so $\theta_o = 6^\circ$ and $\mu = 0.31$ are used as baseline values for the inter-rotor phasing. To match the trim condition, the mean rolling moments for the simulation are targeted directly from the measured values resulting in a slight offset in the mean total loads. Overall the simulation does a good job of capturing the significant factors of the experiment.

A number of prominent features can be identified in Figure 15a. First, this is fixed frame rolling moment so there is a large $2/\text{rev}$ vibratory component, in both the experiment and the simulation, that arises as each blade moves to the advancing side and takes a majority of the lift. The rolling moment when the blades are aligned over the nose and tail of the helicopter is small by comparison. The total system rolling moment is the sum of both the upper and the lower rotor. Trim is achieved when the rotors are balanced, so the mean total rolling moment is close to zero. The $2/\text{rev}$ component of the rolling also cancels.

There is a small oscillation at 90° and 270° , evident in both the independent rotor loads and the combined rotor loads, that is a result of each rotor interacting with its own wake. It can be seen clearly in the independent and total loads when $\phi = 0^\circ$ as the two impulses combine. When the rotor phase is shifted, these interactions move for the phase shifted rotor and the two interactions no longer line up. This

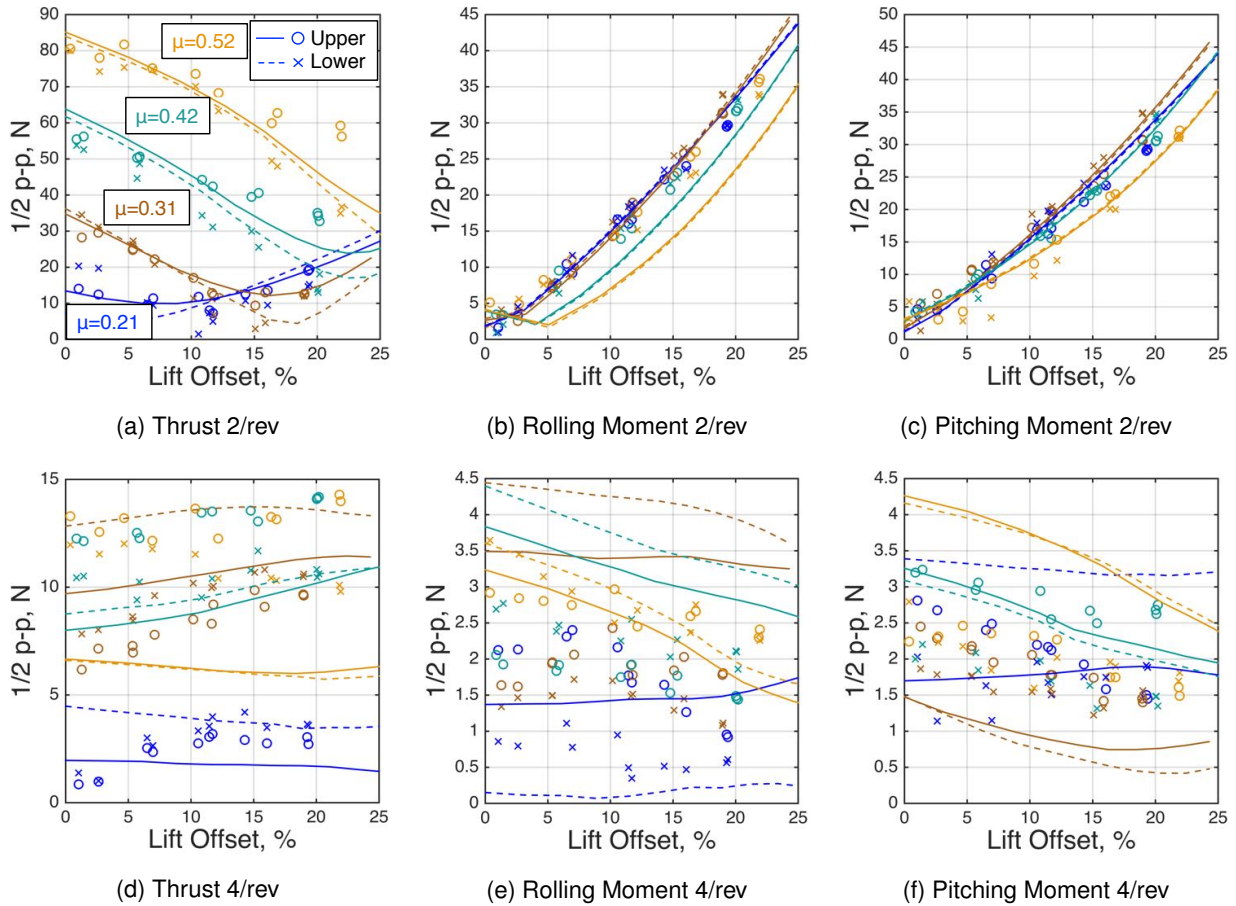


Figure 17: Rotor hub harmonics vs lift offset. ($\theta_o = 6^\circ$)

reduces the clarity of the signal in the total system loads. Finally it is possible to observe a 1/rev oscillation that is present in the experiment but not in the simulation.

5.3.1. Lift Offset

Vibratory hub load trends with lift offset are easiest of the three sources listed to quantify, they are present in isolated rotor lift offset tests and can be seen in consistent behaviors of the coaxial tests. Figure 17 shows how the 2/rev and 4/rev harmonics vary with lift offset and advance ratio for a rotor with $\theta_o = 6^\circ$. The graphs shown for hub loads are limited to thrust, pitching moment and rolling moment. Torque is not included because there is poor agreement between vibrations in the experiment and the simulation, similar to that seen in the steady torque (Figure 9). The in-plane vibratory loads are omitted for a different reason, earlier works demonstrated that there was poor prediction of steady side forces. Further analytical work suggested a coupling between hub moments and in-plane forces in the dynamic calibration. It is currently being evaluated but puts correlations with in-

plane forces in question.

Figure 17a shows that at low lift offset values there is significant 2/rev variation in thrust that tends to decrease with lift offset for all but the lowest advance ratio. This has a direct physical explanation. To achieve zero lift offset at high advance ratios on any rotor, an interesting lift distribution results. The retreating side is limited in the total thrust it can produce by retreating blade stall and low dynamic pressure, requiring the application of high lateral cyclic. As a result, the blade is at a moderate angle over the nose and tail of the rotor, a low angle of attack on the advancing side and has low dynamic pressure on the retreating side. Therefore, the rotor produces a majority of its lift over the nose and tail, Figure 18a, time histories of the thrust is also included. With increasing lift offset the advancing side of the rotor carries more and more lift, this changes the lift distribution seen by each blade from 2/rev to 1/rev which results in a reduction of overall 2/rev thrust, Figure 18b. Lower advance ratios also have significantly lower 2/rev vibrations because these loads are a direct result of attempting to trim at high advance ratios.

Both 2/rev pitching and rolling moment vibrations

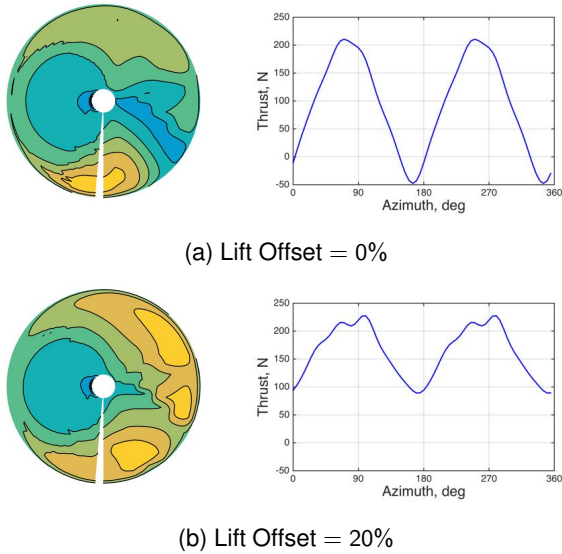


Figure 18: Upper rotor aerodynamic thrust distribution and vertical hub load time history. ($\mu = 0.52$; $\theta_o = 6^\circ$)

are a result of lift offset. In the rotating frame the hub sees a 1/rev rolling moment. When resolved into the fixed frame this produces a rolling moment that has a high mean and 2/rev vibrations, Figure 17b, and a pitching moment with zero mean and high 2/rev vibration, Figure 17c. The slight curvature in these graphs is a result of the increasing thrust with lift offset. If they were plotted against mean rolling moment they would be closer to linear. It is also worth remembering that rotor thrust decreases with increasing advance ratio which is why the rolling moment vibrations tend to decrease slightly with advance ratio.

The 4/rev vibrations show a less clear trend with advance ratio. For thrust, Figure 17d, the 4/rev component increases with advance ratio up to a point but it is not significantly affected by lift offset. The simulation captures the relative value of the vibrations but it seems to exaggerate the difference between the upper and lower rotors. It is expected that the lower rotor would have larger high frequency harmonics because the upper rotor operates in a mostly clean wake, while there is the possibility of more significant wake interactions from the upper rotor on the lower rotor. The pitching, Figure 17e, and rolling moments, Figure 17f show similar behavior. The general magnitude of the 4/rev is represented by the simulation, but the exact values are not captured. It is interesting to note that whereas the thrust showed very little consistent trend with lift offset, the pitching and rolling moment do show a decrease in 4/rev with lift offset, particularly at high advance ratio.

5.3.2. Aerodynamic Interactions

Aerodynamic interaction are challenging to evaluate in a complex system like a coaxial rotor. For isolated rotors, changing the phase has no significant meaning, it only changes the reference time. For well separated tandem rotors with limited interactions the total resulting hub loads will change with phase, but the relative magnitude of the individual rotor harmonics will not. For a coaxial rotor, variations in independent loads with phase must exclusively be the result of aerodynamic interaction Figure 19 shows how each of the 6 primary vibratory loads (same as previously examined) change with phase angle. Two lift offset values are shown, lift offset $\approx 0\%$ and lift offset $\approx 17\%$. Those are only approximate values because it is not possible to guarantee that each point is at the exact lift offset. Reviewing Figure 17 shows that while sweeps with lift offset are well populated there is some scatter in the actual lift offset values captured during each experimental sweep as well as some scatter in the resulting loads. Additionally, only 3 distinct phase angles were examined by the experiment. It is challenging to identify features that are true underlying trends and what are the result of scatter in the data.

The 2/rev pitching, Figure 19b, and rolling moment, Figure 19c, vary little with phase angle, although there is some variation in the experiment. Compared to the magnitude of these harmonics, any variations are relatively small. Clearly, for the high lift offset case there is a large vibratory moment and the phase is set fairly directly by the requirements of trim. The thrust shows larger variations with phase angle, in both the experiment and the analysis. As previously discussed, low lift offset thrust has higher 2/rev harmonics than high lift offset. For the high lift offset case, the simulations captures the change with phase more accurately than it does at low lift offset

The 4/rev harmonics, correlate less well with the simulation, are of lower magnitude overall and show some more pronounced trends with phase. The thrust and rolling moment follow similar trends, although in opposite directions. One rotor tends to decrease and then increase with phase angle while the other increases first and then decreases.

5.3.3. Total Hub Loads

When combining upper and lower rotors, it has been observed that coaxial rotors in hover perform more like a rotor with the same total number of blades ($2 \times N_b$), rather than a tandem rotor with the same number of blades but twice the disk area. The difference is that while hub loads for a 4-bladed rotor will filter our harmonics not related to $4 \times N_b$, the coaxial rotor selectively cancels or doubles the magnitude of even the 2/rev depending on phasing. Figure 15 shows how for the rolling moment for a high lift offset

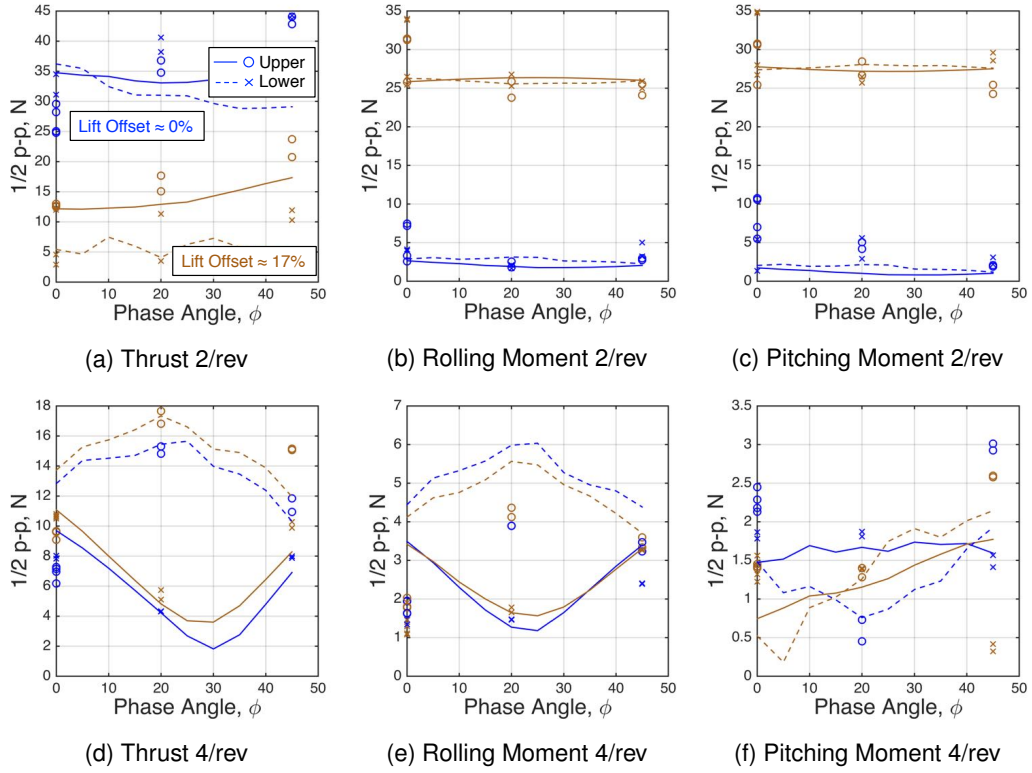


Figure 19: Characteristic harmonics varying with phase.

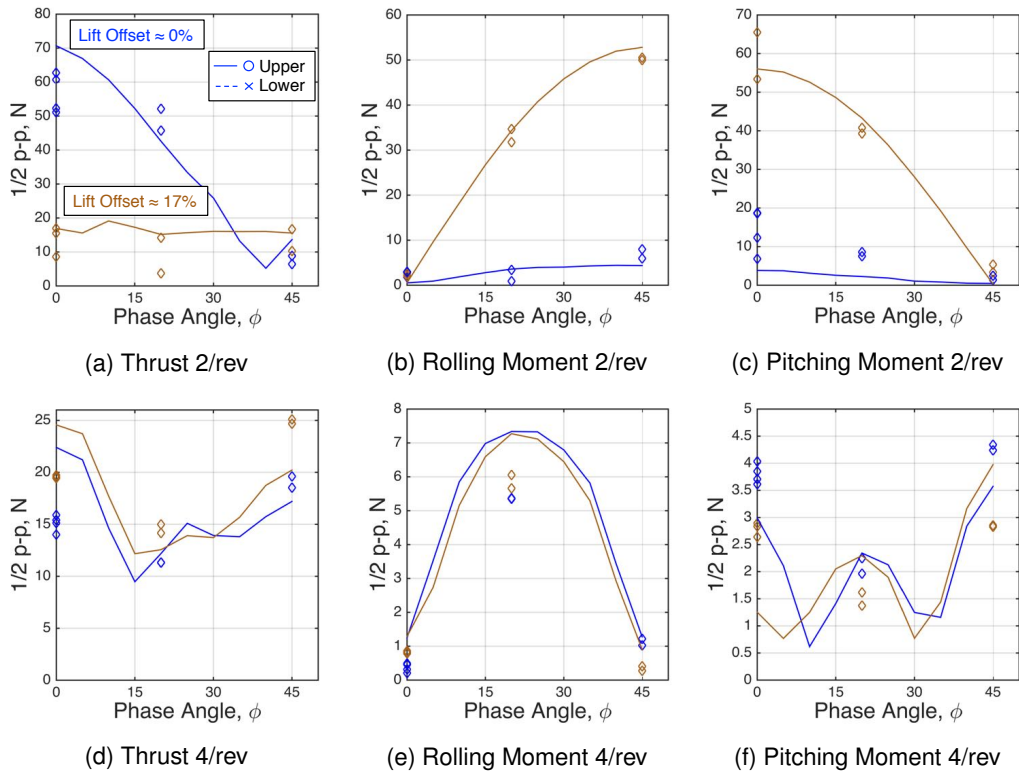


Figure 20: Characteristic harmonics varying with phase and lift offset for the combined system.

case adds together. The upper and lower rotor both have a strong 2/rev component, corresponding to a blade picking up lift on the advancing side. These moments are equal and opposite, so the resulting mean rolling moment is close to zero, which is the goal of a trimmed rotor.

A simple analysis can provide basic insight into how rotor phasing changes the total hub loads. The hub loads from the upper and lower rotor are broken down into the harmonic components and assumed to be similar. An important observation to make is that drag force for both rotors pointing in the direction of the flow while side force points in opposite directions. Mathematically, this is expressed in Equations 3 and 4, the cosine component of every harmonic is in the same direction, while the sine component has the opposite sine.

$$(3) \quad F(\psi^U)^U = \sum_k A_{kS} \sin(k\psi^U) + A_{kC} \cos(k\psi^U)$$

$$(4) \quad F(\psi^L)^L = \sum_k -A_{kS} \sin(k\psi^L) + A_{kC} \cos(k\psi^L)$$

$$(5) \quad \psi^U = \psi + \phi; \quad \psi^L = \psi - \phi$$

$$F(\psi)^U + F(\psi)^L = \sum_k 2 \cos(k\psi)(A_{kS} \sin(k\phi) + A_{kC} \cos(k\phi))$$

(6) Equation 6 illustrates how the phase angle and the harmonic content of the original wave form work together to create the total hub load. The only remaining term to contain the azimuth is $\cos k\psi$, showing that the final waveform has the same integer harmonic value, k , and only consists of cosines, whether the original signal had sines or cosines. There is also a coefficient of 2 at the front of the equation, the maximum potential magnitude of a signal has been doubled. Finally, it can be seen that the magnitude is governed by $A_{kS} \sin(k\phi) + A_{kC} \cos(k\phi)$, meaning that the value of ϕ governs whether the final result is dominated by the original A_{kS} or A_{kC} . For example, in all the earlier experiments, $\phi = 0^\circ$, which results in contribution from only A_{kC} while for the experiments performed at 45° , only contributions from A_{kS} will be present.

6. CONCLUSIONS

A refined comprehensive analysis of a new coaxial rotor wind tunnel experiment was performed. Correlation with the experimental data agrees well in many cases but a few areas have been identified for improvement.

- i Rotor thrust and lift-to-drag ratio are well captured for different speeds.

- ii The ratio of upper to lower rotor thrust, for a torque balanced coaxial rotor, inverts with increasing speed as the upper rotor wake convects off the lower rotor.
- iii 2/rev vibratory thrust is shown to be the result of an uneven thrust distribution that is alleviated through the application of lift offset.
- iv 2/rev vibratory pitch and roll hub moments are a result of the periodic rotating frame moments that result in steady lift offset.
- v The current simulation captures the general trends of the 4/rev vibrations but is less accurate in prediction of magnitude.
- vi Independent rotor loads against rotor-to-rotor phase angle provides an indication of how well the simulation captures the interactional aerodynamics. For the current simulation, the correlation is weak, particularly for 4/rev.
- vii Total coaxial hub loads with rotor-to-rotor phase are well captured using the current methods.

7. ACKNOWLEDGMENTS

The work presented was supported by the VLRCOE program with technical monitor Dr. Mahendra Bhagwat. The authors would like to thank their partners at the UT Austin, particularly Dr. Jayant Sirohi and graduate students Mr. Christopher Cameron and Mr. Daiju Uehara for the opportunity to participate in the wind tunnel testing and data analysis. Dr. Anand Saxena and Dr. VT Nagaraj and the Glenn L Martin Wind Tunnel staff provided invaluable assistance setting up and performing the wind tunnel experiments. We acknowledge Dr. Hyeonsoo Yeo from Army-AFDD for his help in refining the prediction methodology, Tom Maier from AFDD and Oliver Wong from AFDD-Langley for their many helpful insights on model testing, and Rajneesh Singh for his expertise on coaxial simulations. The patient help and insight of Dr. Graham Bowen-Davies, Dr. Ananth Sridharan, Dr. Bharath Govindarajan, and Dr. Anubhav Datta is also greatly appreciated.

References

- [1] Harrington, R. D., "Full-Scale-Tunnel Investigation of the Static-Thrust Performance of a Coaxial Helicopter Rotor," NACA TN 2318, 1951.
- [2] Dingeldein, R. C., "Wind-Tunnel Studies of the Performance of Multirotor Configurations," NACA TN 3236, 1954.

- [3] Coleman, C. P., "A Survey of Theoretical and Experimental Coaxial Rotor Aerodynamic Research," NASA TP 3675, 1997.
- [4] Ramasamy, M., "Hover Performance Measurements Toward Understanding Aerodynamic Interference in Coaxial, Tandem, and Tilt Rotors," *Journal of the American Helicopter Society*, Vol. 60, (3), 2015, pp. 1–17.
- [5] Ruddell, A. J., "Advancing Blade Concept (ABC) Development," American Helicopter Society 32nd Annual Forum, Washington, DC, 1976.
- [6] Felker, F. F., "Performance and Loads Data from a Wind Tunnel Test of a Full-Scale Coaxial, Hingeless Rotor Helicopter," NASA-TM-81329, 1981.
- [7] Walsh, D., Weiner, S., Arifian, K., Lawrence, T., Wilson, M., Millott, T., and Blackwell, R., "High Airspeed Testing of the Sikorsky X2 Technology TM Demonstrator," American Helicopter Society 67th Annual Forum, Virginia Beach, VA, 2011.
- [8] Blackwell, R. and Millott, T., "Dynamics Design Characteristics of the Sikorsky X2 Technology TM Demonstrator Aircraft," American Helicopter Society 64th Annual Forum, Fort Worth, TX, 2008.
- [9] Leishman, J. G., *Principles of Helicopter Aerodynamics*, Cambridge University Press, New York, NY, 2000.
- [10] Johnson, W., *Rotorcraft Aeromechanics*, Cambridge University Press, New York, NY, 2013.
- [11] Rand, O. and Khromov, V., "Aerodynamic Optimization of Coaxial Rotor in Hover and Axial Flight," 27th International Congress of the Aeronautical Sciences, Nice, France, 2012.
- [12] Juhasz, O., Syal, M., Celi, R., Khromov, V., Rand, O., Ruzicka, G. C., and Strawn, R. C., "Comparison of Three Coaxial Aerodynamic Prediction Methods Including Validation with Model Test Data," *Journal of the American Helicopter Society*, Vol. 59, (3), Jul 2014, pp. 1–14.
- [13] Yeo, H., Field, M., and Johnson, W., "Investigation of Maximum Blade Loading Capability of Lift-Offset Rotors," *Journal of the American Helicopter Society*, Vol. 59, (1), 2014.
- [14] Johnson, W., Elmore, J. F., Keen, E. B., Galaher, A. T., and Nunez, G. F., "Coaxial Compound Helicopter for Compound Urban Operations," American Helicopter Society Technical Meeting on Aeromechanics Design for Vertical Lift, San Francisco, CA, January 2016.
- [15] Lakshminarayan, V. K. and Baeder, J. D., "High-Resolution Computational Investigation of Trimmed Coaxial Rotor Aerodynamics in Hover," *Journal of the American Helicopter Society*, Vol. 54, (4), 2009, pp. 042008.
- [16] Singh, R., Kang, H., Bhagwat, M., Cameron, C., and Sirohi, J., "Computational and Experimental Study of Coaxial Rotor Steady and Vibratory Loads," 54th AIAA Aerospace Sciences Meeting, San Diego, CA, January 2016.
- [17] Passe, B. and Baeder, J. D., "Computational Investigation of Coaxial Rotor Interactional Aerodynamics in Steady Forward Flight," 33rd AIAA Applied Aerodynamics Conference, Dallas, TX, June 2015.
- [18] Cameron, C., Uehara, D., and Sirohi, J., "Transient Hub Loads and Blade Deformation of a Mach-Scale Coaxial Rotor in Hover," Kissimmee, FL, January 2015.
- [19] Cameron, C. and Sirohi, J., "Performance and Loads of a Model Coaxial Rotor Part I : Wind Tunnel Testing Department of Aerospace Engineering and Engineering," American Helicopter Society 72nd Annual Forum, West Palm Beach, FL, 2016.
- [20] Chopra, I. and Bir, G., "University of Maryland Advanced Rotor Code: UMARC," American Helicopter Society Aeromechanics Specialists Conference, San Francisco, CA, January 1994.
- [21] Schmaus, J. and Chopra, I., "Aeromechanics for a High Advance Ratio Coaxial Helicopter," January, American Helicopter Society 71st Annual Forum, Virginia Beach, VA, May 5-7 2015.
- [22] Schmaus, J. and Chopra, I., "Performance and Loads of a Model Coaxial Rotor Part II: Prediction Validations with Measurements," American Helicopter Society 72nd Annual Forum, West Palm Beach, FL, May 17-19 2016.
- [23] Srinivasan, G. R. and Baeder, J. D., "TURNS: A Free-Wake Euler/Navier-Stokes Numerical Method for Helicopter Rotors," *AIAA Journal*, Vol. 31, (5), 1991, pp. 959–962.
- [24] Bagai, A. and Leishman, J. G., "Free-Wake Analysis of Tandem, Tilt-Rotor and Coaxial Rotor Configurations," American Helicopter Society 51st Annual Forum, Fort Worth, TX, 1996.
- [25] Langer, H. J., Peterson, R. L., and Maier, T. H., "An Experimental Evaluation of Wind Tunnel Wall Correction Methods for Helicopter Performance," American Helicopter Society 52nd Annual Forum, Washington, DC, 1996.